Uptake of Gas-Phase Species by 1-Octanol. 1. Uptake of α-Pinene, γ-Terpinene, *p*-Cymene, and 2-Methyl-2-hexanol as a Function of Relative Humidity and Temperature

H. Z. Zhang, Y. Q. Li,† J. R. Xia, and P. Davidovits*

Chemistry Department, Merkert Chemistry Center, Boston College, Chestnut Hill, Massachusetts 02467-3809

L. R. Williams, J. T. Jayne, C. E. Kolb, and D. R. Worsnop

Center for Aerosol and Cloud Chemistry, Aerodyne Research Inc., 45 Manning Road, Billerica, Massachusetts 01821-3976

Received: January 30, 2003; In Final Form: May 26, 2003

With use of a droplet train apparatus, the uptake by 1-octanol of gas-phase α-pinene, γ-terpinene, *p*-cymene, and 2-methyl-2-hexanol was measured as a function of relative humidity and temperature (263−293 K). 1-Octanol was selected as a surrogate for hydrophobic oxygenated organic compounds found in tropospheric aerosols. The mass accommodation coefficients (α) of γ-terpinene, *p*-cymene, and 2-methyl-2-hexanol obtained from these measurements exhibit negative temperature dependences. The upper and lower values of α at 265 and 290 K, respectively, are as follows: for γ-terpinene 0.12 and 0.076; for *p*-cymene 0.20 and 0.097; and for 2-methyl-2-hexanol 0.25 and 0.11. The uptake of α-pinene is solubility limited, yielding values for the product $HD_l^{1/2}$ for α-pinene in 1-octanol (H = Henry's law constant, D_l = liquid-phase diffusion coefficient). With use of estimated values of D_l the Henry's law constant is obtained as $\ln H\ (\mathrm{M/atm}) = -(6.59 \pm 1.16) + (3.80 \pm 0.31) \times 10^3/T$. The presence of water vapor does not affect the uptake of the above organic gas-phase species. Uptakes of the gas-phase species benzene, H_2O, SO_2, and H_2S were also studied and were found to below the detection limit of the droplet apparatus. This implies that the uptake coefficient for these species is less than 10^{-3} for trace gas/liquid droplet interaction times up to 1.5×10^{-2} s.

Introduction

Tropospheric aerosol particles were initially envisioned as consisting mainly of inorganic salts, soot, and/or minerals. Recent field studies have shown that their composition is far more complex. It is now clear that organic compounds are abundant in many regions of the troposphere and represent a significant mass fraction of tropospheric particles. For example, over the continental USA the mass percentage of organic compounds in aerosols is often in the range of 20−50% for particles less than 2.0 μm in diameter.[1,2]

Organic aerosols, as do other aerosols, directly affect the atmospheric radiative budget and are expected to play an important role in the chemistry of the atmosphere.[2] Further, hydrophilic organic aerosols can serve as cloud condensation nuclei, often as effectively as inorganic sulfate aerosols,[2,3] and thus also indirectly affect the atmospheric radiative budget. During the past decade, considerable phenomenological information has been gathered about inorganic aerosols. However, much about the formation, evolution, and important interactions of organic aerosols remains unknown.[2,4]

The composition of organic aerosols is often highly complex, consisting of hundreds of compounds with a large fraction still unidentified.[1,2,5] To obtain basic information about the atmospheric behavior of organics, in the face of such complexity, one must study surrogate compounds representing classes of organic species found in aerosols.[6]

For our first organic liquid studies, we chose ethylene glycol as a surrogate for hydrophilic organic compounds.[7] We measured uptake of gas-phase HCl and HBr on a pure ethylene glycol surface and on ethylene glycol−water mixture surfaces as a function of water mole fraction (0 to 1) under liquid−vapor equilibrium conditions. The uptake studies yielded mass accommodation and thermal accommodation coefficients, and provided information about the nature of hydrophilic organic surfaces as a function of relative humidity.

In the present study, 1-octanol was selected as a surrogate for hydrophobic oxygenated organic compounds. Octanol was chosen as a surrogate compound for several reasons. While octanol is not a significant component of atmospheric particles, it shares properties with some organic compounds found in such aerosols. Like octanol, the alcohols linalool and 4-terpineol, and caprylic and stearic acids are all polar and are only slightly soluble in water. Further, 1-octanol has been used as a model aerosol compound in several experiments that studied aerosol−air and aerosol−water partitioning coefficients for volatile and semivolatile organic compounds.[8−13] Finally, in experiments such as ours, which require a significant amount of the liquid, cost is a factor.

Octanol is a hydrophobic, oily, low vapor pressure liquid. (Vapor pressures at 273 and 298 K are 0.005 and 0.079 Torr, respectively.) The solubility of 1-octanol in water is low. (At 298 K the mole fraction solubility is 7.45×10^{-5}.[14]) On the other hand, the solubility of water in octanol is significantly higher. At 298 K the mole fraction solubility of water is 0.27.[14,15]

† Current address: Atmospheric Sciences Research Center, State University of New York, 251 Fuller Road, Albany, NY 12203.

10.1021/jp0342529 CCC: $25.00
Published on Web 07/30/2003

(The corresponding equilibrium water vapor pressure at that point is close to that of pure water.)

With use of a droplet train apparatus, two sets of uptake studies were performed with 1-octanol. In the first set of studies, reported in this article, uptakes of the organic gas-phase species α-pinene, γ-terpinene, *p*-cymene, and 2-methyl-2-hexanol by 1-octanol were measured as a function of relative humidity (R.H.) and temperature (263−293 K). With the exception of 2-methyl-2-hexanol, these are monoterpenes emitted into the atmosphere by various evergreen trees.[16−18] In a fir forest, the atmospheric concentration of monoterpenes was observed to be as high as 2.9 ppbv.[19] The oxidative products of these molecules are important components of organic aerosols. The molecule 2-methyl-2-hexanol was added to the study as a convenient surrogate for biogenic alcohols, such as 2-methyl-3-buten-2-ol (MBO),[20] (3*Z*)-hexenol,[21] and *n*-hexanol,[22] which are also emitted by evergreens and certain types of oak.

In the second set of studies, the uptake coefficients of gas-phase HCl, HBr, HI, and acetic acid were measured to probe the nature of hydrophobic organic surfaces as a function of relative humidity and temperature. While the measured uptake of the organic gas-phase species is in accord with expectations, the observed uptake of the gas-phase acids, as is described in the following companion article, is quite surprising.

Gas−Liquid Interactions

In the droplet train apparatus, described in the following section, a gas-phase species interacts with liquid droplets and the disappearance of that species from the gas phase is monitored. A phenomenological description of the entry of gases into liquids is straightforward. First, the gas-phase molecule is transported to the liquid surface, usually by gas-phase diffusion. The initial entry of the species into the liquid is governed by the mass accommodation coefficient, α.

In the absence of surface reactions, the mass accommodation coefficient determines the maximum flux, *J*, of gas into a liquid, which is given by:

$$J = \frac{n_g \bar{c} \alpha}{4} \tag{1}$$

Here n_g is the density of the gas molecules of interest and $\bar{c}$ is their average thermal speed. If reactions occur at the gas−liquid interface, then the flux of species disappearing from the gas phase may exceed that given by eq 1. Of course, the flux cannot exceed the collision rate $(n_g\bar{c})/4$.

In a laboratory experiment, gas uptake by the liquid is usually limited by gas-phase diffusion and, in the absence of rapid surface and/or liquid-phase reactions, can also be limited by solubility constraints as the species in the liquid approaches Henry's law saturation. In the latter process, some of the molecules that enter the liquid evaporate back into the gas phase due to the limited solubility of the species. As expected, this effect increases with gas−liquid interaction time. At equilibrium, the liquid is saturated and the flux of molecules into the liquid is equal to the rate of desorption of these molecules out of the liquid. The net uptake is then zero. Chemical reactions of the solvated species in the bulk liquid can provide a sink for the species, reducing the effect of saturation, and this increases the species uptake from the gas phase. In experiments subject to these effects, the measured flux (*J*) into a surface is expressed in terms of a measured uptake coefficient, γ_{meas}, as:

$$J = \frac{n_g \bar{c} \gamma_{meas}}{4} \tag{2}$$

The challenge in experimental trace gas/liquid interaction studies is to design techniques to deconvolute the processes involved in the overall gas uptake, allowing the mass accommodation coefficient, and other fundamental parameters of interest, to be determined.

General solutions to the uptake flux equations (eq 2), which include the coupled effects of gas-phase diffusion, mass accommodation, Henry's law solubility, and chemical reactions (if any), are not available. However, solutions under various restricted conditions have been presented in the literature.[23,24] On the basis of the available analytical solutions, approximate expressions for gas uptake have been formulated in which the various processes are decoupled.

As noted above the first process to occur is gas-phase transport of the trace species to the gas/liquid interface. To our knowledge, gas-phase diffusive transport of a trace gas to a train of moving droplets, as used in many of our experiments,[25−31] has not been treated analytically. In fact, gas-phase diffusive transport even to a single stationary droplet does not lend itself to a straightforward analytical solution over the range of Knudsen numbers covering the continuum and transition flow regimes. However, an empirical formulation of diffusive transport to a stationary droplet developed by Fuchs and Sutugin[32] has been shown to be in good agreement with experimental data.[33]

The Fuchs−Sutugin formulation can be written as a resistance equation that decouples gas diffusion and interfacial processes,[34−36] such that

$$\frac{1}{\gamma_{meas}} = \frac{1}{\Gamma_{diff}} + \frac{1}{\gamma_0} \tag{3}$$

Here the parameter Γ_{diff} takes into account the effect of gas-phase diffusion on the uptake, and γ_0 is the uptake coefficient in the limit of "zero pressure", i.e., in the absence of any gas-phase diffusion limitation. In the Fuchs−Sutugin formulation for a stationary droplet, Γ_{diff} is

$$\frac{1}{\Gamma_{diff}} = \frac{0.75 + 0.283\mathrm{Kn}}{\mathrm{Kn}(1 + \mathrm{Kn})} \tag{4}$$

Here, Kn is the Knudsen number defined as $2\lambda/d$, where λ is the gas-phase mean free path, *d* is the diameter of the particle, and D_g is the gas-phase diffusion coefficient of the species. The mean free path is here expressed as $\lambda = 3D_g/\bar{c}$.

An extensive set of experiments reviewed by Worsnop et al.[30] has shown that with a simple modification, the Fuchs−Sutugin formulation also provides a good representation of diffusive transport to a train of closely spaced moving droplets. In the modified expression, *d* in the definition of Kn is replaced by an effective diameter for the diffusive process, d_f, given by $d_f = (2.0 \pm 0.1)d_o$, where d_o is the diameter of the droplet-forming orifice. The principal features of the diffusive transport model as used in our work have been recently derived theoretically by Sugiyama et al.[37] and Morita et al.[38]

The parameter γ_0 accounts for the effects on the gas uptake of the mass accommodation coefficient, Henry's law solubility, and liquid and surface reactions, if any. Because of solubility limitations, γ_{meas} is, in general, a function of the gas−liquid interaction time.

It is possible to obtain a simple approximate expression for γ_0 by de-coupling from each other the effects of mass accommodation and solubility. In such a simplified representation, the uptake coefficient Γ_{sat} takes into account the effects on the uptake of Henry's law solubility[39] (see note, ref 39). In the

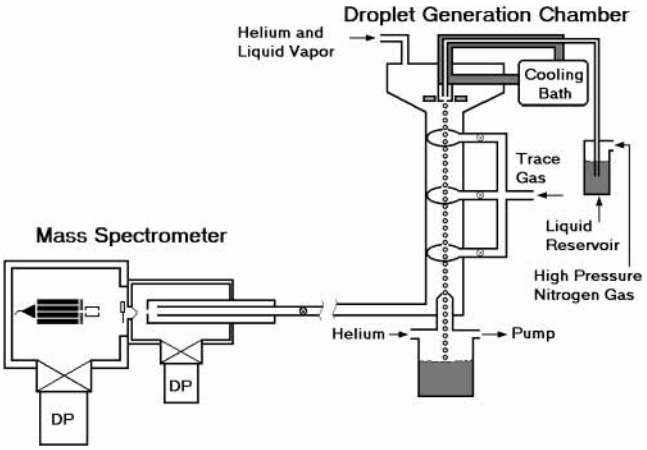

Figure 1. Schematic of the droplet train flow reactor apparatus. A description is found in the text. (Reprinted with permission from Nathanson et al., 1996; Copyright 1996, American Chemical Society.)

present studies, chemical reactions of the gas-phase species with the liquid do not occur, and therefore γ_0 can be expressed as,

$$\frac{1}{\gamma_0} = \frac{1}{\alpha} + \frac{1}{\Gamma_{sat}} \tag{5}$$

The parameter Γ_{sat} is given by[29]

$$\frac{1}{\Gamma_{sat}} = \frac{\bar{c}}{8RTH}\sqrt{\frac{\pi t}{D_l}} \tag{6}$$

where D_l is the liquid-phase diffusion coefficient of gas-phase molecules in the liquid, t is the gas−liquid interaction time, R is the gas constant (L atm/(K mol)), T is temperature, and H (M atm^{-1}) is the Henry's law constant. Note that Γ_{sat} measures the extent to which the gas-phase species is out of equilibrium with the liquid. As equilibrium is approached, Γ_{sat} approaches 0.

The above decoupled formalism leads to a resistor model in which $1/\gamma_0$ is represented as an electrical circuit with $1/\alpha$ connected in series to $1/\Gamma_{sat}$. The resistor circuit for the measured uptake (i.e. $1/\gamma_{meas}$) is then the series combination of $1/\Gamma_{diff}$ and $1/\gamma_0$ as in eq 3.[29] The separability of the processes represented by these parameters has been verified by our experimental results.[25−29,31]

Experimental Description

In the droplet train apparatus shown in Figure 1,[29,40] a fast-moving monodisperse, spatially collimated train of droplets is produced by forcing a liquid through a vibrating orifice located in a separate chamber. In this experiment the liquid is 1-octanol obtained at 99% stated purity from Sigma-Aldrich Inc. The speed of the liquid droplets is in the range of 1500−2800 cm s^{-1} determined by the pressure of the gas that forces the liquid through the orifice, and the orifice diameter. The droplet train is passed through a ~30 cm long, 1.4 cm diameter, longitudinal low-pressure (2−19 Torr) flow reactor that contains the trace gas species, in this case α-pinene, γ-terpinene, *p*-cymene, or 2-methyl-2-hexanol at a density between 2×10^{13} and 3×10^{14} cm^{-3}. The flow tube wall is heated to about 50 °C to improve the stability of the experiment. However, the data are independent of wall temperature tested from 25 to 100 °C.

The trace gas is entrained in a flowing mixture of an inert gas (usually helium) and 1-octanol vapor at equilibrium pressure with the liquid 1-octanol droplets. The trace gas is introduced through one of three loop injectors located along the flow tube. By selecting the gas inlet port and the droplet velocity, the gas−droplet interaction time can be varied between about 2 and 15 ms.

Depending on the frequency of orifice vibration and the liquid flow rate, the 70- and 30-μm-diameter orifices used in this study generate droplets of diameter in the range of 150−300 and 60−130 μm, respectively. Droplet formation frequencies range from 8 to 48 kHz. The uniformity of the droplets and the droplet velocity along the flow tube are monitored by passing cylindrically focused He−Ne laser beams through the droplet train at three heights along the flow tube.[30] The droplet velocity along the flow tube is measured to be constant to within 3%. Note that these droplets are large enough that their curvature has a negligible effect on the equilibrium vapor pressure.

The diameter, and hence the surface area of the droplets passing through the flow tube is changed in a stepwise fashion by changing the driving frequency applied to the piezo ceramic in contact with the droplet-forming orifice. The density of the trace gas is monitored with a quadrupole mass spectrometer. The uptake coefficient (γ_{meas}) as defined by eq 2 is calculated from the measured change in trace gas signal via eq 7.[40] Here

$$\gamma_{meas} = \frac{4F_g}{\bar{c}\Delta A} \ln \frac{n_g}{n_g'} \tag{7}$$

F_g is the carrier-gas volume flow rate (~100 to 500 cm^3 s^{-1}) through the system, $\Delta A = A_1 - A_2$ is the change in the total droplet surface area in contact with the trace gas, and n_g and n_g' are the trace gas densities at the outlet of the flow tube after exposure to droplets of area A_2 and A_1, respectively.

An important aspect of the experimental technique is the careful control of all the conditions within the apparatus, especially the 1-octanol vapor pressure in the droplet generation chamber and in the flow tube. Experiments with 1-octanol were performed between 263 and 293 K where the equilibrium 1-octanol vapor pressure varies from 0.0015 to 0.048 Torr depending on temperature. The liquid 1-octanol delivery lines were cooled to the desired droplet temperature. The temperature of the droplets in the reaction zone is maintained by introducing a partial pressure of 1-octanol equal to the equilibrium vapor pressure at the droplet temperature.[40] The required equilibrium 1-octanol vapor is produced by bubbling helium gas through the liquid 1-octanol in a temperature-controlled bubbler and flowing the gas into the droplet generation region at the entrance of the flow tube reactor.

To conduct gas uptake studies as a function of relative humidity, a known amount of water vapor is introduced into the droplet generation region at the entrance of the flow tube reactor. Water vapor is produced by bubbling helium carrier gas through liquid water contained in a temperature-controlled vessel. The helium in the flow tube is at a partial pressure between 2 and 6 Torr, depending on experimental conditions.

The equilibrium relationship between the water vapor pressure (P_{H_2O}) and the liquid mole fraction of water (X_{H_2O}) in the 1-octanol−water solution was obtained from the work of Apelblat[41] and Marcus[14] as described in Appendix 1. From these studies, we obtain P_{H_2O} as a function of X_{H_2O} as displayed in Figure 2. The equilibrium water vapor pressures for pure water at 267, 273, and 283 K are 2.93, 4.58, and 9.21 Torr, respectively, and are indicated by arrows in the figure.

In our first studies of the effect of relative humidity on gas uptake, droplets were formed from octanol−water solutions at a water concentration set to be in equilibrium with the water

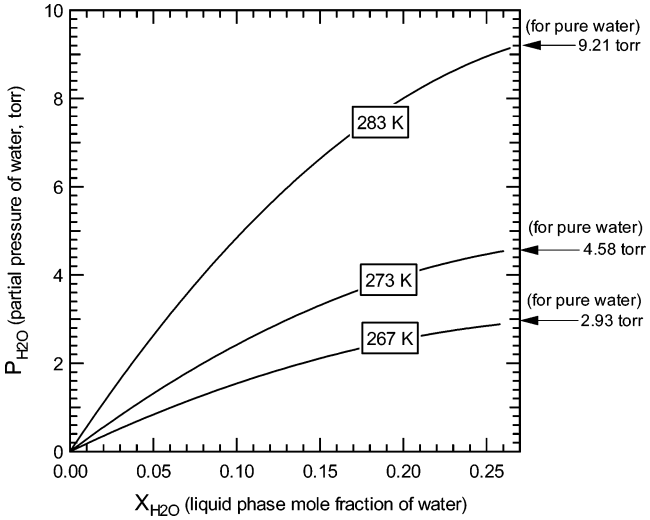

Figure 2. Partial pressure of water vapor (P_{H_2O}, Torr) as a function of liquid-phase mole fraction of water (X_{H_2O}) in the 1-octanol−water binary system at 267, 273, and 283 K (see Appendix 1).

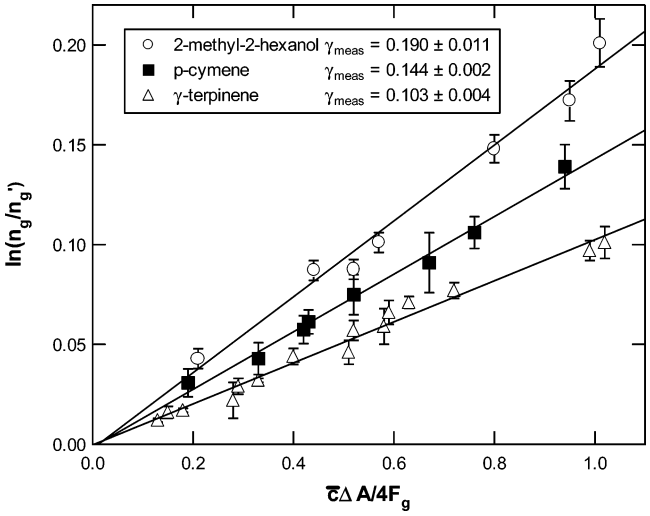

Figure 3. Experimental data showing plots of $\ln(n_g/n_g')$ as a function of $\bar{c}\Delta A/4F_g$ for γ-terpinene (Δ) at droplet temperature $T_d = 267$ K and for *p*-cymene (■) and for 2-methyl-2-hexanol (○) at $T_d = 275$ K. Solid lines are the least-squares fit to the data. The slope of the lines is γ_{meas}. Terms are defined in the text.

vapor in the flow tube in accord with the calculations in Appendix 1 and Figure 2. Experiments with the organic vapors as well as with gas-phase acids (see the following article) showed that the gas uptake is the same with droplets formed from pure octanol and exposed to water vapor or from equilibrium octanol−water solutions. This indicates that the near surface region of the droplet reaches equilibrium with the water vapor during the transit time between the droplet-forming orifice and the first trace gas injector loop (about 10 ms). Because experimental procedures are significantly simplified, most of the relative humidity studies were performed with droplets initially formed of pure octanol.

Overall pressure balance in the flow tube was checked by monitoring simultaneously both the trace species studied and the concentration of an inert reference gas, in this case Xe. This gas is effectively insoluble in the liquid droplets. Any change in the reference gas concentration with droplet switching determines the "zero" of the system and was subtracted from observed changes in trace gas concentration. In the present experiments this correction was always less than 5%.

Results and Analysis

As an example of experimental data, we show in Figure 3 a plot of $\ln(n_g/n_g')$ at R.H. = 0 for γ-terpinene (267 K), *p*-cymene (275 K), and 2-methyl-2-hexanol (275 K) as a function of $\bar{c}\Delta A/4F_g$. Here $\bar{c}\Delta A/4F_g$ was varied by changing the gas flow rate and the droplet surface area (ΔA). Each point in the figure is the average of at least 10 area change cycles and the error bars represent one standard deviation from the mean in the experimental $\ln(n_g/n_g')$ value. As is evident from eq 7, the slope of the plots in Figure 3 yields the value of γ_{meas}, in this case with a precision of ~5%. These data yield $\gamma_{meas} = 0.103$, 0.144, and 0.190 for γ-terpinene (at 267 K), *p*-cymene, and 2-methyl-2-hexanol (at 275 K), respectively. The precision for these measurements is also indicated in the figure. Similar plots were obtained for a wide range of experimental parameters, for which the uptake fraction, $(n_g - n_g')/n_g$ varied from 3% to 50%.

The effect of gas-phase diffusion on the uptake is taken into account by Γ_{diff} calculated from eq 4. Here the gas-phase diffusion coefficient D_g (see Table 1 for numerical values) used to calculate Kn is estimated by using the method described by Reid et al.[42] The temperature of the gas for the D_g calculation was assumed to be the average between the wall temperature and the droplet surface temperature (see Worsnop et al.[40]).

TABLE 1: Gas-Phase Diffusion Coefficients, D_g (atm cm^2 s^{-1}), Estimated at 298 K

	carrier gas	
trace gas	He	H_2O
2-methyl-2-hexanol	0.311	0.092
p-cymene	0.275	0.086
α-pinene	0.211	0.081
γ-terpinene	0.211	0.081

The parameter γ_0, the uptake coefficient in the absence of gas-phase diffusion limitation, is then obtained via eq 3. To minimize the effect of gas-phase diffusion, uptake is usually measured at the lowest overall gas pressure consistent with the required equilibrium vapor pressure of the droplets and the necessary inert carrier gas flow. However, in most of our studies we validate our treatment of gas-phase diffusive transport by measuring trace gas uptake as a function of increasing inert gas background pressure, and with different inert gases, significantly changing the Knudsen number. As noted, droplet-forming orifices of two diameters were used (30 and 70 μm), generating droplet diameters ranging from 60 to 300 μm. The uptake coefficient γ_{meas} for γ-terpinene at 276 K as a function of Kn is shown in Figure 4. The solid line is a plot of eq 3 with Γ_{diff} given by eq 4. As is evident, our formulation of gas-phase diffusion provides a good fit to the experimental data. The asymptote at large Kn, designated as γ_0, is the uptake coefficient in the limit of "zero pressure", i.e., in the absence of gas-phase diffusion limitation. (In the absence of solubility limitation or surface reaction, $\gamma_0 = \alpha$.) These gas-phase diffusion studies are in accord with previous experiments conducted with sulfuric acid and water droplets.[30,43]

In previous experiments with water and aqueous acid droplets we tested the validity of our formulation of Γ_{diff} over a wide range of Kn values.[30] However, in those experiments we could not simply add water vapor to test the effect of decreasing Kn, because water vapor itself affects the uptake properties and the surface temperature of aqueous liquids. In the present uptake studies on octanol, water vapor is simply an inert gas. In these studies, γ_0 is in the range 0.1−0.2 and in the usual set up, with about 7 Torr of He as the carrier gas, Kn ~ 1.2, and $1/\Gamma_{diff}$ is

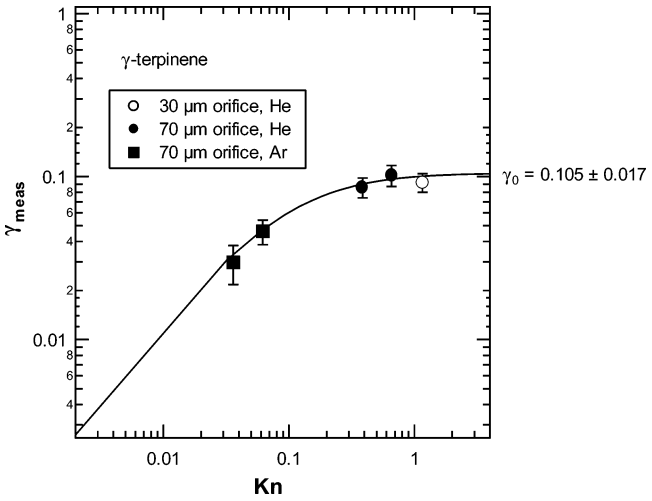

Figure 4. Uptake coefficient γ_{meas} as a function of Knudsen number (Kn) for γ-terpinene at 276 K. Open symbol data were obtained with the 30-μm droplet-forming orifice; filled symbol data were obtained with the 70-μm orifice. Data obtained with argon carrier gas are shown as squares; data obtained with helium carrier gas are shown as circles. The solid line is the best fit to the data via eq 3 with Γ_{diff} given by eq 4.

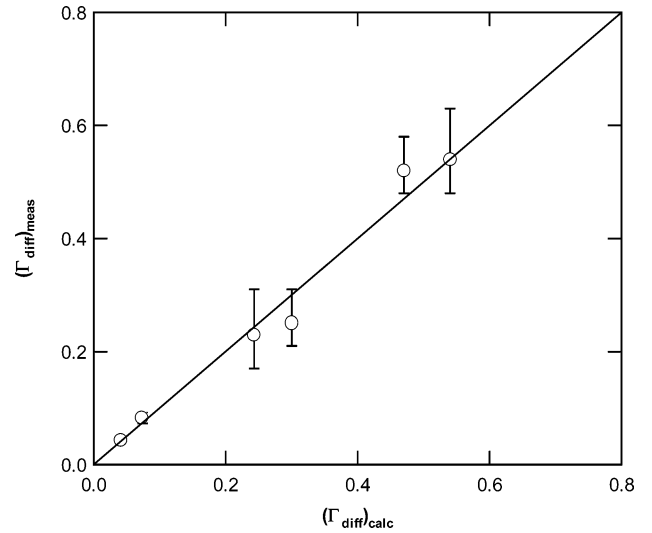

Figure 5. The diffusion parameter $(\Gamma_{diff})_{meas}$ obtained from measurements as discussed in the text plotted versus $(\Gamma_{diff})_{calc}$ obtained from eq 4. See Table 2 for experimental parameters.

about 0.4. Under these conditions the correction for diffusive transport is less than 10% [i.e. $(\gamma_0 - \gamma_{meas})/\gamma_0$]. Water vapor is added and a measured $(\Gamma_{diff})_{meas}$ is computed from $1/(\Gamma_{diff})_{meas} = 1/\gamma_{meas} - 1/\gamma_0$. The diffusion parameter $(\Gamma_{diff})_{meas}$ is then plotted vs the value of the calculated $(\Gamma_{diff})_{calc}$ obtained from eq 4. A combined plot for γ-terpinene, α-pinene, and *p*-cymene with argon and helium carrier gases is shown in Figure 5. Values for the relevant parameters related to the numbered points in the figure are listed in Table 2. They include the partial pressures of the carrier gases, Kn, γ_0, and γ_{meas}. The diameter of the droplet-forming orifice in these experiments was 70 μm. The correlation between $(\Gamma_{diff})_{meas}$ and $(\Gamma_{diff})_{calc}$ is 0.988.

In Figure 6, γ_0 values for γ-terpinene on octanol at 276 K are plotted as a function of gas−droplet contact time at 0% and 90% relative humidity, open and solid square symbols, respectively (at 90% R.H. water vapor pressure = 5.1 Torr). As is evident, on the scale of the experimental gas−liquid interaction times the uptake of gas-phase γ-terpinene is time independent, that is, $1/\Gamma_{sol}$ is negligible compared to $1/\alpha$.

TABLE 2: Values for the Relevant Parameters Related to the Numbered Points in Figure 5[a]

data	P_{tot} (Torr)	P_{H_2O} (Torr)	Kn	γ_0	γ_{meas}
1[a]	29.2[I]	3.1	0.030	0.105 ± 0.017	0.030 ± 0.002
2[a]	17.8[I]	5.3	0.054	0.105 ± 0.017	0.046 ± 0.003
3[b]	11.5[II]	4.3	0.166	0.116 ± 0.013	0.077 ± 0.008
4[b]	6.1[II]	4.1	0.201	0.116 ± 0.013	0.079 ± 0.005
5[c]	7.3[II]	3.4	0.300	0.201 ± 0.022	0.145 ± 0.003
6[a]	9.1[II]	0.0	0.340	0.105 ± 0.017	0.088 ± 0.002

[a] Data points in Figure 5 are in the above order from left to right. Key: a = γ-terpinene; b = α-pinene; c = *p*-cymene; I = argon; II = helium.

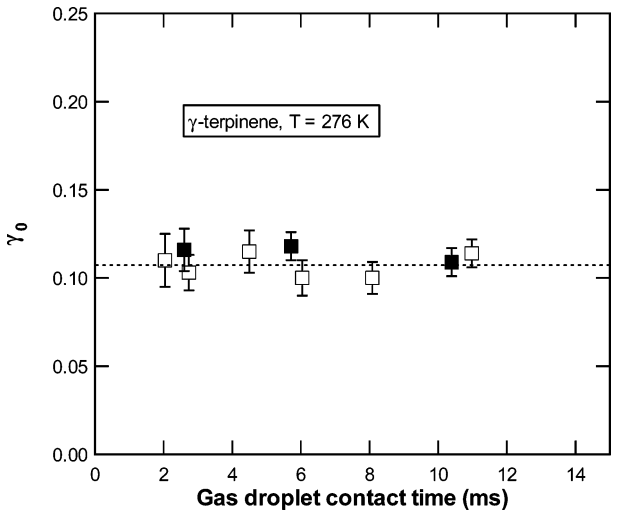

Figure 6. Uptake coefficient γ_0 for γ-terpinene as a function of gas−liquid contact time at droplet temperature T_d = 276 K. R.H. = 0 (□); R.H. = 90% (5.10 Torr water vapor pressure) (■). The dashed line is the best straight-line fit to the data.

Therefore, for γ-terpinene $\gamma_0 = \alpha$. Likewise, the uptake is independent of relative humidity (R.H.). Similar plots were obtained at all other temperatures studied. The uptakes of *p*-cymene and 2-methyl-2-hexanol are likewise time independent of the scale of the experimental gas−liquid interaction times. The mass accommodation coefficients (α) as a function of temperature for γ-terpinene, *p*-cymene, and 2-methyl-2-hexanol are shown in Figure 7 and the data are tabulated in Table 3. The accuracy of these results, determined principally by uncertainties in flow rate measurements, is estimated to be about ±15% as indicated in the table.

By contrast, the uptake coefficient γ_0 for α-pinene is time dependent as shown in Figure 8. Here γ_0, at 273 K, is plotted as a function of gas−droplet contact time. The uptake was measured under three conditions: (1) pure octanol droplets R.H. = 0 (○); (2) initially pure octanol droplets R.H. = 94% (4.10 Torr water vapor pressure) (●); and (3) octanol−water solution droplets with $X_{H_2O} = 0.2$ (liquid mole fraction of water) and corresponding equilibrium water vapor pressure 3.99 Torr (R.H. = 87%) (■). As is evident, uptake of α-pinene does not depend on relative humidity but is clearly a function of gas−droplet contact time indicating a solubility limited uptake. The solid line in the figure is a plot of Γ_{sat} as given by eq 6.

The coefficients *H* and D_l for α-pinene in eq 6 have not been measured independently. Therefore, the product $HD_l^{1/2}$ was a variable in the fitting of the experimental points. The best fit to the data in Figure 8 at 273 K was obtained with $HD_l^{1/2} = 1.32$ M cm/(atm $s^{1/2}$). Similar plots were obtained at the other temperatures studied, yielding $HD_l^{1/2} = 1.65, 0.90, 0.65$ M cm/(atm $s^{1/2}$) at 263, 283, and 293 K, respectively.

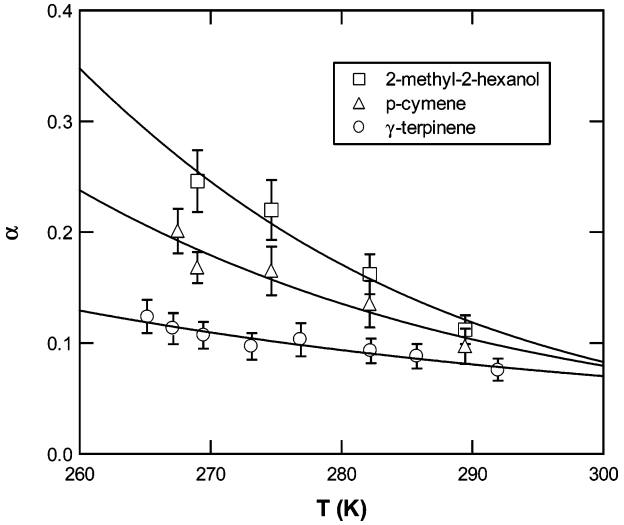

Figure 7. Mass accommodation coefficients (α) for γ-terpinene (○), *p*-cymene (Δ), and 2-methyl-2-hexanol (□) on 1-octanol as a function of temperature. Solid lines are obtained via eq 10 with ΔH_{obs} and ΔS_{obs} values listed in Table 3.

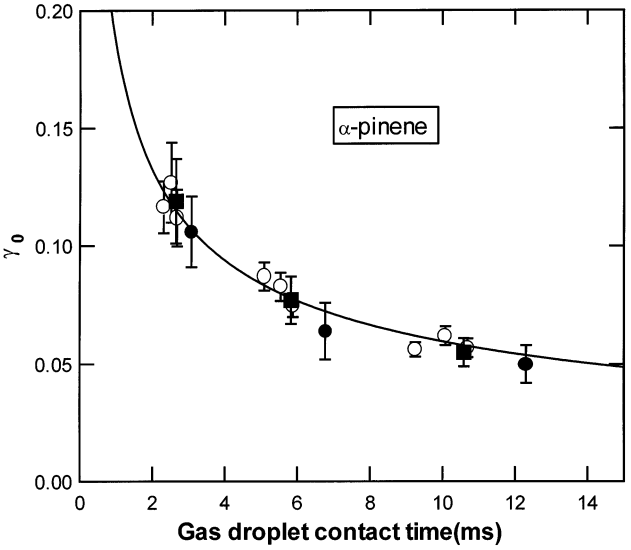

Figure 8. Uptake coefficient γ_0 for α-pinene as a function of gas−liquid contact time at droplet temperature $T_d = 273$ K. The uptake was measured under three conditions: (1) pure octanol droplets R.H. = 0 (○); (2) initially pure octanol droplets R.H. = 94% (4.10 Torr water vapor pressure) (●); and (3) octanol−water solution droplets with $X_{H_2O} = 0.2$ (liquid mole fraction of water) and corresponding equilibrium water vapor pressure 3.99 Torr (R.H. = 87%) (■). The solid line is the best fit to the data via eq 5, with Γ_{sat} given by eq 6.

TABLE 3: The Mass Accommodation Coefficients (α) for γ-Terpinene, *p*-Cymene, and 2-Methyl-2-hexanol at the Temperatures Shown Corresponding to Figure 7

T (K)	α		
	γ-terpinene	*p*-cymene	2-methyl-2-hexanol
265	0.124 ± 0.015		
267	0.113 ± 0.014	0.201 ± 0.020	
269	0.107 ± 0.012	0.168 ± 0.021	0.246 ± 0.028
273	0.097 ± 0.012		
275	0.103 ± 0.015	0.165 ± 0.022	0.220 ± 0.027
282	0.093 ± 0.011	0.135 ± 0.014	0.162 ± 0.018
286	0.088 ± 0.011		
290	0.076 ± 0.010	0.097 ± 0.016	0.112 ± 0.013

While the diffusion coefficient D_l of α-pinene in octanol has not been measured, a value for this parameter can be calculated from the Hayduk−Minhas correlation.[42] The calculation method is outlined in Appendix 2. With use of these values for D_l, the Henry's law coefficients *H* were computed from the measured values of $HD_l^{1/2}$. The measured values of $HD_l^{1/2}$ and the computed values of D_l and *H* are listed in Table 4. A best fit to the *H* values in Table 4 yields the following expression for *H* (*T* in K).

TABLE 4: Values of $HD_l^{1/2}$, D_l, and *H* for α-Pinene as a Function of Temperature

T (K)	$HD_l^{1/2}$ (M cm atm^{-1} s$^{-1/2}$)	D_l (cm^2 s^{-1})	*H* (M atm^{-1})
263	1.65 ± 0.09	3.95×10^{-7}	$(2.55 \pm 0.37) \times 10^3$
273	1.32 ± 0.10	6.46×10^{-7}	$(1.64 \pm 0.27) \times 10^3$
283	0.90 ± 0.60	1.01×10^{-6}	$(8.93 \pm 1.39) \times 10^2$
293	0.65 ± 0.11	1.53×10^{-6}	$(5.21 \pm 1.39) \times 10^2$

$$\ln H\,(\mathrm{M/atm}) = -(6.59 \pm 1.16) + (3.80 \pm 0.31) \times 10^3/T \quad (8)$$

Because solubility limitation dominates the α-pinene uptake, our experiments do not yield an accurate value for the α-pinene mass accommodation coefficient. Only a lower limit for α can be extracted from the uptake data. The uptake of α-pinene was measured at four temperatures: 263, 273, 283, and 293 K. An error analysis yields a lower limit of α at these temperatures of 0.30, 0.25, 0.21, and 0.10, respectively. However, α could be as high as 1 at all temperatures studied.

Uptake of the gas-phase species benzene, H_2O, SO_2, and H_2S was also studied and was found to be below the detection limit of the droplet apparatus. This implies that the uptake coefficient, γ_{meas}, for these species is less than 10^{-3} for trace gas/liquid droplet interaction times up to 1.5×10^{-2} s.

Discussion

Mass Accommodation. As is shown in Figure 7, the mass accommodation coefficients for γ-terpinene, *p*-cymene, and 2-methyl-2-hexanol show a negative temperature dependence. A negative temperature dependence of α was observed in our previous uptake studies conducted with 30 or so hydrophilic gas-phase species including alcohols, hydrogen peroxide, and acetone on aqueous surfaces,[31] as well as HCl, HBr, DCl, and H_2O on ethylene glycol surface.[7] These results are consistent with the following formulation of mass accommodation that was developed for the mass accommodation of gas molecules on water.

Mass accommodation can be viewed as a two-step process involving surface adsorption followed by a competition between desorption and solvation as shown in eq 9.[31,44]

$$n_g \underset{k_{des}}{\overset{k_{ads}}{\rightleftharpoons}} n_s \xrightarrow{k_{sol}} n_l \quad (9)$$

First, the gas molecule strikes the surface and is thermally accommodated. It has been shown that at relatively low energies the thermal accommodation coefficient is close to unity.[45,46] With this assumption, the adsorption rate constant is $k_{ads} = \bar{c}/4$. This adsorbed surface species then either enters the liquid (rate constant k_{sol}) or desorbs (rate constant k_{des}) from the surface. Evaporation of the species out of the bulk liquid is taken into account separately, via the term Γ_{sat} in eq 6. The mass accommodation coefficient (α) is then shown to be[44]

$$\frac{\alpha}{1-\alpha} = \frac{k_{sol}}{k_{des}} = \frac{\exp(-\Delta G_{sol}/RT)}{\exp(-\Delta G_{des}/RT)} = \exp\left(\frac{\Delta G_{obs}}{RT}\right) \quad (10)$$

The parameter $\Delta G_{obs} = \Delta H_{obs} - T\Delta S_{obs}$ is the Gibbs energy of

TABLE 5: ΔH_{obs} and ΔS_{obs} for γ-Terpinene, *p*-Cymene, and 2-Methyl-2-hexanol

	ΔH_{obs} (kcal mol^{-1})	ΔS_{obs} (cal mol^{-1} K^{-1})	N^*
2-methyl-2-hexanol	$-(6.87 \pm 0.92)$	$-(27.7 \pm 3.3)$	1.5
p-cymene	$-(4.42 \pm 1.17)$	$-(19.5 \pm 4.2)$	1.3
γ-terpinene	$-(2.63 \pm 0.34)$	$-(13.9 \pm 1.2)$	1.2

the transition state between molecules in the gas phase and molecules solvated in the liquid phase. The values for ΔH_{obs} and ΔS_{obs} can be obtained from the experimental results by plotting $\ln(\alpha/(1-\alpha))$ as a function of $1/T$. The slope of such a plot is $-\Delta H_{obs}/R$ and the intercept is $\Delta S_{obs}/R$. The ΔH_{obs} and ΔS_{obs} values for γ-terpinene, *p*-cymene, and 2-methyl-2-hexanol are listed in Table 5.

The functional form of ΔG_{obs} depends on the theoretical formulation of the uptake process. Therefore, the parameter ΔG_{obs} serves as a bridge between experiment and theory. Uptake studies on water surfaces led to the formulation of a nucleation critical cluster model for mass accommodation that successfully explained several features noted in our earlier uptake studies on aqueous surfaces including the observation that a plot of ΔH_{obs} versus ΔS_{obs} for all the species studied exhibits a straight-line relationship.[44,46] The ΔH_{obs} and ΔS_{obs} values for the three molecules studied here likewise form a straight line with a slope about 30% higher than observed for the aqueous surfaces. This observation suggests that the nucleation model of mass accommodation may also apply to the organic 1-octanol surface. As will be seen, in keeping with the nucleation critical cluster model of gas uptake, the difference in the water and octanol slopes is simply due to the difference in the parameters determining the energetics of nucleation.

In the nucleation critical cluster model of mass accommodation the gas−liquid surface is envisioned as a dynamic region where due to thermal fluctuations, small clusters or aggregates of liquid molecules are expected to be continually forming, falling apart, and re-forming. Therefore, the driving force is such that clusters smaller than a critical size (N^*) fall apart, whereas clusters larger than the critical size serve as centers for further condensation and grow in size until they merge into the adjacent bulk liquid. In this model, gas uptake proceeds via such growth of critical clusters. The incoming gas molecule upon striking the surface becomes a loosely bound surface species (n_s) that participates in the surface nucleation process. If such a molecule becomes part of a critical size cluster that grows, it will invariably be incorporated into the bulk liquid via cluster growth.[44,46]

In this model, the ease with which a molecule can be incorporated into bulk liquid depends on its ability to enter the nucleation or aggregation process with the molecules of the liquid at the interface. The critical cluster consists of a specific number of molecules N^*, which is the sum of the trace molecule plus the additional number of molecules of the liquid substance required to form the critical cluster or aggregate leading to growth and subsequent uptake by the bulk liquid. This number N^* required to form a critical cluster depends on the structure of the specific molecule undergoing the uptake process.

The incoming molecule, once adsorbed in the interface surface region, can be found in various aggregate configurations. However, since the gas-phase species under consideration consists primarily of monomers, detailed balance considerations lead to the conclusion that molecules of the species leave the interface primarily as monomers via the breakage of an interfacial bond associated with the most weakly bound unaggregated species, n_s. Therefore, it seems reasonable to assume

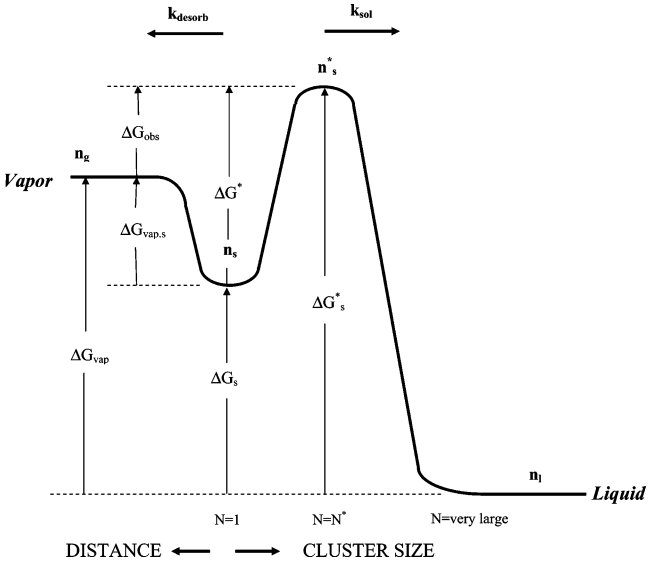

Figure 9. Postulated free energy diagram for the liquid vapor interface. Note the change in reaction coordinate at $N = N^*$ (see text). The experimentally measured ΔG_{obs} corresponds to the difference in energy between the vapor (n_g) and surface transition state (n^*_s). Negative ΔH_{obs} and ΔS_{obs} values imply that the n^*_s barrier is entropic in nature, with the barrier height determined by the critical cluster size (N^*). The mass accommodation kinetics are controlled by the relative rates of k_{desorb} and k_{sol}. (Reprinted with permission from Nathanson et al., 1996; Copyright 1996, American Chemical Society.)

that the uptake process involves primarily only two of the various interfacial configurations of the trace molecule; the most weakly interconnected species, n_s, and the species within a critical cluster, n^*_s. The free energies with respect to the bulk liquid for these two species are ΔG_s and ΔG^*_s. A postulated free energy diagram for the relevant species in the region between liquid and gas is shown in Figure 9 (reproduced with permission from Nathanson et al.[44,46]).

One has to be careful in interpreting the reaction coordinate in Figure 9. To the left of the n_s minimum, the reaction coordinate represents the distance between the trace gas molecule and the interface. However, to the right of this minimum, distance is no longer a well-defined quantity. The trace molecule is now within the interface. We suggest that here the appropriate reaction coordinate is the number size (N) of the aggregate containing the trace molecule. Thus at the n_s minimum $N = 1$. As N increases, the free energy first increases and then, past the critical size (i.e. $N = N^*$), the free energy decreases and the cluster grows until it merges with the bulk liquid. In Figure 9, ΔG_{obs}, the experimentally measured free energy, corresponds to the difference between ΔG_{vap} and ΔG^*_s, the free energies of the vapor (n_g) and the critical cluster (n^*_s), respectively. As shown in Figure 9, $\Delta G_{vap,s} = [\Delta G_{vap} - \Delta G_s]$ is the free energy of the gas-phase species, n_g, with respect to the surface species, n_s.

The model formulation of critical cluster nucleation invokes transition state theory to account for the barrier at n^*_s that controls observed accommodation kinetics. We note that, since ΔH_{obs} and ΔS_{obs} are always both negative, the free energy barrier at n^*_s is entropic in nature. In the model formulation, formation of the critical cluster is always favored enthalpically; the negative entropic term reflects dissolution of the vapor into liquid, with a large contribution due to the surface tension of small clusters. Note that the kinetics within the interface, represented by the diagram in Figure 9, serves as a bridge between the vapor and the liquid phases. Interfacial transport,

characterized by α, is distinct from bulk phase transport that is controlled by solubility and diffusion.

In our previous work we presented a quantitative formulation for the nucleation critical−cluster model of mass accommodation, using simple nucleation theory. The formulation yielded expressions for ΔH_{obs} and ΔS_{obs} as[44,46]

$$\Delta H_{obs} = (N^* - 1)\Delta H_c + (N^{*2/3} - 1)\left[4\pi E_s N_{Av}\left(\frac{3V_m}{4\pi N_{Av}}\right)^{2/3}\right] - \Delta H_{vap.s} \quad (11)$$

$$\Delta S_{obs} = (N^* - 1)[\Delta S_c + R\ln(p/MRT)] + (N^{*2/3} - 1)\left[4\pi S_s N_{Av}\left(\frac{3V_m}{4\pi N_{Av}}\right)^{2/3}\right] - \Delta S_{vap.s} \quad (12)$$

The parameters ΔH_c and ΔS_c are related to the free energy of condensation for the liquid under consideration, in this case octanol ($\Delta G_c = \Delta H_c - T\Delta S_c$). That is, ΔG_c is the free energy of transferring a mole of gas-phase octanol into liquid octanol without volume change rather than the usually tabulated standard free energy of condensation. The parameters ΔH_c and ΔS_c are only slightly temperature dependent and for octanol at 25 °C they are $\Delta H_c = -18$ kcal/mol and $\Delta S_c = -34$ cal M^{-1} K^{-1}, tabulated in the paper by Ben-Naim and Marcus.[47] The parameters E_s and S_s are related to surface tension β expressed as $\beta = E_s - TS_s$. Surface tension for octanol as a function of temperature was obtained from data compilation by Daubert and Danner,[48] yielding $E_s = 1.2 \times 10^{-6}$ cal cm^{-2} and $S_s = 1.9 \times 10^{-9}$ cal cm^{-2} K^{-1}. Formally, in classical nucleation theory, the parameter p in eq 12 is the vapor pressure of the nucleating species in the region where the nucleation is occurring. In the present application we reinterpret p to make the expression in eq 12 meaningful at the gas−liquid interface. Accordingly, here we regard p as an equivalent 1-octanol density ($p = nRT$) in the surface region where the incoming trace molecule collides with the interface, and is adsorbed. To simplify the fitting procedure we will use the same value for p as was determined from fits to data for aqueous surfaces,[46] i.e., $p = 67$ Torr, $R\ln(p/MRT) = -15$ for octanol. In our calculations we assume that $\Delta G_{vap.s} = f_1 \times \Delta H_c - f_2 \times \Delta S_c T$. (Note that ΔG_{vap} is the negative of the free energy of condensation, i.e., $\Delta G_{vap} = -\Delta G_c$.)

Equations 11 and 12 now contain two unknown parameters: f_1 and f_2. Our strategy is to obtain values for f_1 and f_2 for selected values of N^* so as to provide a fit to the set of experimental data in Table 5. A good fit to the experimental data is obtained with $f_1 = 0.10$, $f_2 = 0.27$. With these and other previously discussed numerical values for the relevant parameters we obtain,

$$\Delta H_{obs} = -18(N^* - 1) + 14.3(N^{*2/3} - 1) - 0.10 \times 18 \text{ (kcal } M^{-1}) \quad (13)$$

$$\Delta S_{obs} = -34(N^* - 1) - 15(N^* - 1) + 22.7(N^{*2/3} - 1) - 0.27 \times 34 \text{ (cal } M^{-1}\ K^{-1}) \quad (14)$$

Calculated values of ΔH_{obs} and ΔS_{obs} for selected values of N^* are shown in Table 6. These values together with the measurements are plotted in the Figure 10. The values of N^* for the organic gases studied are also shown in Table 5. The dashed line in the figure is the calculated $\Delta H_{obs} - \Delta S_{obs}$ relationship for water.[44,46] For the purpose of future discussion, we also show in the figure experimental values of ΔH_{obs} and ΔS_{obs} for acetic acid presented in the following companion article.[49] As is evident, the formulations for ΔH_{obs} and ΔS_{obs} in eqs 13 and 14 for the organic gases as well as acetic acid are in accord with the measurements.

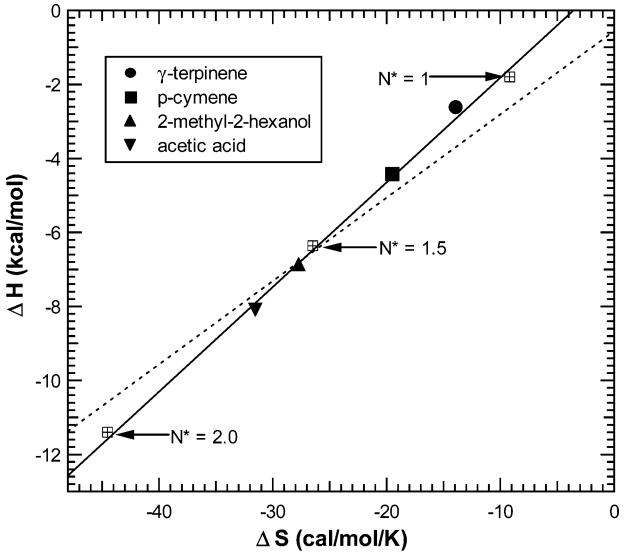

Figure 10. Experimental and calculated values of ΔH_{obs} and ΔS_{obs}: γ-terpinene (solid circle); *p*-cymene (solid square); 2-methyl-2-hexanol (triangle); acetic acid (inverse triangle); cand alculations (crossed square). The dashed line in the figure is the calculated $\Delta H_{obs} - \Delta S_{obs}$ relationship for water.

TABLE 6: Calculated Values for ΔH_{obs} and ΔS_{obs} Obtained via Eqs 13 and 14

N^*	ΔH_{obs} (kcal mol^{-1})	ΔS_{obs} (cal mol^{-1} K^{-1})
1.0	−1.8	−9.2
1.5	−6.4	−26
2.0	−11	−45
2.5	−17	−63

Clearly individual critical clusters must contain an integer number of molecules. However, for a given trace molecule the number of octanol molecules required to form a critical cluster ($N^* - 1$) may depend on the orientation of the trace molecule with respect to the bulk liquid and its penetration into the interfacial region. We interpret noninteger N^* values as representing an average number of molecules in a critical cluster or aggregate in the interfacial region. For example, in the case of 2-methyl-2-hexanol, where the measured values of ΔH_{obs} and ΔS_{obs} are best matched with $N^* = 1.5$, the critical-sized cluster consists of the molecule itself with either one or two octanol molecules aggregated with it, depending on its position and orientation within the interfacial region.

We expect that the number of octanol molecules required to form a critical cluster (with a given trace gas) will depend inversely on the attraction between the trace gas and octanol. (That is, the trace gas that exerts the largest attractive force will be associated with the smallest N^*.) This expectation is supported by the results show in Table 5. The molecular weights of γ-terpinene, *p*-cymene, and 2-methyl-2-hexanol are 136, 134, and 116, respectively, and the vapor pressures are 1.1, 1.5, and 2.1 Torr at 298 K. The attractive forces exerted by organics on each other are commonly proportional to molecular weight and inversely proportional to vapor pressure. (We assume here that self-attraction (determining the vapor pressure) is proportional to the attraction of the molecule to octanol.) The N^* values in Table 5 are ordered accordingly. That is, the molecule with

the largest molecular weight and smallest vapor pressure (γ-terpinene) displays the lowest N^*.

Finally we note that the quantitative formulation of the mass accommodation process yielding the values of N^* in Table 6 entails several assumptions and approximations. (This is discussed in previous publications.[44,46]) Therefore, the values for N^* in the table are not to be considered as accurate representations of the critical cluster size at the interface. Rather, the listing shows the relative ordering of N^* and it illustrates that N^* is relatively small. However, the actual critical cluster size could be significantly larger, say 4 or 5.

Effect of Relative Humidity on Liquid Octanol. As was pointed out, the mass accommodation coefficients for γ-terpinene, *p*-cymene, and 2-methyl-2-hexanol, as well as the product $HD_l^{1/2}$ for α-pinene, are independent of water vapor density (i.e. independent of the mole fraction of water in liquid octanol). This is not surprising, because there is evidence that neither the relevant surface nor the bulk properties are altered significantly by the water content of octanol at levels present in our experiments (<0.2 mol fraction). First, we measured the surface tension of octanol at 298 K, as a function of mole fraction of water. Within the experimental accuracy of the measurement (∼5%), the surface tension remained un-altered up to about 0.27 mol fraction of water (corresponding to a saturated solution at 298 K). This result is consistent with the experiments of Ishida et al.,[50] who measured the surface tension of a lithium bromide aqueous solution as a function of added 1-octanol. They found that adding as little as 10^{-5} mol fraction of octanol to the solution reduced the surface tension from that of pure water to that of pure octanol (72.8 dyn/cm to 27.5 dyn/cm). These results indicate that the surface of octanol−water solutions consists predominantly of octanol molecules.

There is also evidence that the liquid-phase diffusion coefficient of octanol (D_l), is not changed substantially by the addition of water. Model calculations of DeBolt et al.[51] performed at 40 °C show that that the addition of an equilibrium amount of water to octanol increases self-diffusion from $(0.68 \pm 0.01) \times 10^{-5}$ cm^2 s^{-1} to $(0.70 \pm 0.01) \times 10^{-5}$ cm^2 s^{-1}, an increase of only about 3%. The calculations are within about a factor of 2 of the measured values.[52]

While there is no direct information about the value of H as a function of added water, the following considerations would lead one to conclude that this parameter likewise remains substantially unaltered. Dallas and Carr[53] measured the free energy of transfer for 11 alcohols into pure and water-saturated octanol. They concluded that "the water is almost completely associated with 1-octanol and scarcely effects the properties of the media."

Atmospheric Implications. Our measurements show that hydrophobic organic gas-phase species have a relatively large mass accommodation coefficient on octanol (at 273 K α is in the range 0.1−0.3). As was the case for aqueous liquids, here also the mass accommodation coefficient exhibits a negative temperature dependence. Even though α is large, under some conditions it may still be the limiting factor in the growth of octanol-like aerosols. As is evident from eqs 3 and 5, the uptake of highly soluble gas-phase species by aerosols is a function of the mass accommodation α and gas-phase diffusion uptake coefficients (Γ_{diff}). The parameter α limits the uptake rate when $\alpha < \Gamma_{diff}$. At 1 atm, the diffusion uptake coefficient (Γ_{diff}) is greater than 0.1 for particles smaller than 2.5 μm. Therefore for aerosols of such size α will affect uptake. Realistic modeling of aerosol/particle interactions with organic gases of the type studied in this work should utilize accurate values of the mass accommodation coefficient.

Appendix 1: Partial Pressure of Water Over a Water−Octanol Solution

As was mentioned in the text, water is partially soluble in 1-octanol. Here we present an expression relating the liquid mole fraction of water in the 1-octanol−water solution to the equilibrium water vapor pressure. The water vapor pressure (P_{H_2O}) in equilibrium with the 1-octanol−water solution can be expressed in terms of the equilibrium vapor pressure of pure water ($P^o_{H_2O}$) and the activity of water in the 1-octanol−water solution (a_{H_2O}) as[14]

$$P_{H_2O} = P^o_{H_2O} \times a_{H_2O} \qquad \text{(A1-1)}$$

The water activity (a_{H_2O}) as a function of liquid mole fraction of water (X_{H_2O}) between 0.05 and 0.27 was measured at 298 K by Apelblat.[41] In this range a_{H_2O} increases from 0.28 to 1 and its values can be fit (in this range only) to within 2% accuracy by the expression

$$a_{H_2O} = 6.17X_{H_2O} - 9.13(X_{H_2O})^2 \qquad \text{(A1-2)}$$

The temperature dependence of a_{H_2O} has not been measured. However, over the temperature range of the present studies, a_{H_2O} is not expected to deviate significantly from eq A1-2. (Typically, activity coefficients change by only a few percent for a 10-deg change in temperature.[42]) Combining eq A1-1 and eq A1-2, we obtain (again in the range of $X_{H_2O} = 0.05$ to 0.27)

$$P_{H_2O} = P^o_{H_2O} \times [6.17X_{H_2O} - 9.13(X_{H_2O})^2] \qquad \text{(A1-3)}$$

Figure 2 in the text shows a plot of this equation at the three temperatures of the present study.

Appendix 2: Diffusion Coefficients of α-Pinene in 1-Octanol

The Hayduk−Minhas expression (eq A2-1) for the diffusion coefficient in nonaqueous solutions is given by Reid et al.[42]

$$D_l = 1.55 \times 10^{-8} \frac{1}{V_B^{0.23}} \frac{T^{1.29}}{\eta_b^{0.92}} \frac{P_b^{0.50}}{P_a^{0.42}} \qquad \text{(A2-1)}$$

Where D_l (cm^2/s) is the mutual diffusion coefficient of solute **a** (here, α-pinene) in solvent **b** (here, 1-octanol). V_B is the molar volume of solvent **b** (1-octanol) at its normal boiling temperature ($T_b = 468.3$ K). (Here, $V_B = 191.3$ cm^3/mol.) η_b is the viscosity of solvent **b** at temperature T. The parameters P_a (for solute) and P_b (for solvent) are expressed in terms of the molar volume V_a (for solute, cm^3/mol) and V_b (for solvent, cm^3/mol), and the surface tension σ_a (for solute, dyn/cm) and σ_b (for solute, dyn/cm) at the required temperatures, respectively, as,

$$P_a = V_a \sigma_a^{1/4}$$

$$P_b = V_b \sigma_b^{1/4}$$

Note that V_B and V_b are not the same. The former is the molar volume at the boiling point and the latter is the molar volume at temperature T. Values for required parameters that are η_b, V_b, σ_b, V_a, and σ_a were obtained from Daubert and Danner[48] and are listed in Table 7.

TABLE 7: Values of Required Parameters for the Calculation of Diffusion Coefficients of α-Pinene in 1-Octanol (Values Obtained from Daubert and Danner (1989))

T (K)	η_b (cP)	V_b (cm^3/mol)	σ_b (dyn/cm)	V_a (cm^3/mol)	σ_a (dyn/cm)
263	32.77	153.5	29.93	154.2	30.06
273	20.24	154.8	29.12	155.5	29.11
283	13.07	156.1	28.32	156.8	28.18
293	8.78	157.5	27.51	158.2	27.24

Equation A2-1 is valid for low concentrations of solute. In the present experiments, the mole fraction of solute is on the order of 10^{-4}. The expression in eq A2-1 has been shown to be accurate to about 15%.[42] Calculated values for the diffusion coefficients of α-pinene in 1-octanol are listed in Table 3.

Acknowledgment. We thank Dr. Erick Swartz for technical input. Funding for this work was provided by the National Science Foundation Grant Nos. ATM-0212464 and CH-0089147, by the Department of Energy Grant No. DE-FG02-98ER62581, and by the US-Israel Binational Science Foundation Grant No. 1999134.

References and Notes

(1) Saxena, P.; Hildemann, L. M. *J. Atmos. Chem.* **1996**, *24*, 57.
(2) Jacobson, M. C.; Hansson, H.-C.; Noone, K. J.; Charlson, R. J. *Rev. Geophys.* **2000**, *38*, 267.
(3) Novakov, T.; Penner, J. E. *Nature* **1993**, *365*, 823.
(4) Andreae, M. O.; Crutzen, P. J. *Science* **1997**, *276*, 1052.
(5) Turpin, B. J.; Saxena, P.; Andrews, E. *Atmos. Environ.* **2000**, *34*, 2983.
(6) Moise, T.; Rudich, Y. *J. Geophys. Res. Atmos.* **2000**, *105*, 14667.
(7) Li, Y. Q.; Zhang, H. Z.; Davidovits, P.; Jayne, J. T.; Kolb, C. E.; Worsnop, D. R. *J. Phys. Chem. A* **2001**, *106*, 1220.
(8) Tse, G.; Sandler, S. I. *J. Chem. Eng. Data* **1994**, *39*, 354.
(9) Bhatia, S. R.; Sandler, S. I. *J. Chem. Eng. Data* **1995**, *40*, 1196.
(10) Harner, T.; Mackay, D. *Environ. Sci. Technol.* **1995**, *29*, 1599.
(11) Harner, T.; Bidleman, T. F. *J. Chem. Eng. Data* **1996**, *41*, 895.
(12) Finizio, A.; Mackay, D.; Bidleman, T.; Harner, T. *Atmos. Environ.* **1997**, *31*, 2289.
(13) Lun, R.; Varhanickova, D.; Shiu, W. Y.; Mackay, D. *J. Chem. Eng. Data* **1997**, *42*, 951.
(14) Marcus, Y. *J. Sol. Chem.* **1990**, *19*, 507.
(15) Schwarzenbach, R. P.; Gschwend, P. M.; Imboden, D. M. *Environmental Organic Chemistry*; John Wiley & Sons: New York, 1993.
(16) Cao, X.-L.; Boissard, C.; Juan, A. J.; Hewitt, C. N.; Gallaher, M. *J. Geophys. Res.* **1997**, *102*, 18903.
(17) Street, R. A.; Owen, S.; Duckham, S. C.; Boissard, C.; Hewitt, C. N. *Atmos. Environ.* **1997**, *31*, 89.
(18) Pio, C. A.; Valente, A. A. *Atmos. Environ.* **1998**, *32*, 683.
(19) Harrison, D.; Hunter, M. C.; Lewis, A. C.; Seakins, P. W.; Bonsang, B.; Gros, V.; Kanakidou, M.; Touaty, M.; Kavouras, I.; Mihalopoulos, N.; Stephanou, E.; Alves, C.; Nunes, T.; Pio, C. *Atmos. Environ.* **2001**, *35*, 4699.
(20) Harley, P.; Fridd-Stroud, V.; Greenberg, J.; Guenther, A.; Vasconcellos, P. *J. Geophys. Res.* [*Atmospheres*] **1998**, *103*, 25479.
(21) Arey, J.; Winer, A. M.; Atkinson, R.; Aschmann, S. M.; Long, W. D.; Morrison, C. L. *Atmos. Environ., Part A* **1991**, *25A*, 1063.
(22) Fall, R. *Reactive Hydrocarbons in the Atmosphere*; Academic Press: San Diego, CA, 1999.
(23) Sherwood, T. K.; Pigford, R. L. *Absorption and Extraction*, 2nd ed.; McGraw-Hill: New York, 1952.
(24) Danckwerts, P. V. *Gas−Liquid Reactions*; McGraw-Hill: New York, 1970.
(25) Jayne, J. T.; Duan, S. X.; Davidovits, P.; Worsnop, D. R.; Zahniser, M. S.; Kolb, C. E. *J. Phys. Chem.* **1991**, *95*, 6329.
(26) Duan, S. X.; Jayne, J. T.; Davidovits, P.; Worsnop, D. R.; Zahniser, M. S.; Kolb, C. E. *J. Phys. Chem.* **1993**, *97*, 2284.
(27) Hu, J.; Shorter, J. A.; Davidovits, P.; Worsnop, D. R.; Zahniser, M. S.; Kolb, C. E. *J. Phys. Chem.* **1993**, *97*, 11037.
(28) De Bruyn, W. J.; Shorter, J. A.; Davidovits, P.; Worsnop, D. R.; Zahniser, M. S.; Kolb, C. E. *J. Geophys. Res.* **1994**, *99*, 16927.
(29) Shi, Q.; Davidovits, P.; Jayne, J. T.; Worsnop, D. R.; Kolb, C. E. *J. Phys. Chem. A* **1999**, *103*, 8812.
(30) Worsnop, D. R.; Shi, Q.; Jayne, J. T.; Kolb, C. E.; Swartz, E.; Davidovits, P. *J. Aerosol Sci.* **2001**, *32*, 877.
(31) Kolb, C. E.; Davidovits, P.; Worsnop, D. R.; Shi, Q.; Jayne, J. T. *Prog. Kinet. Mech.* **2002**, *27*, 1.
(32) Fuchs, N. A.; Sutugin, A. G. *Highly Dispersed Aerosols*; Ann Arbor Science Publishers, available from Butterworth-Heinemann: Newton, MA, 1970.
(33) Widmann, J. F.; Davis, E. J. *J. Aerosol Sci.* **1997**, *28*, 87.
(34) Van Doren, J. M.; Watson, L. R.; Davidovits, P.; Worsnop, D. R.; Zahniser, M. S.; Kolb, C. E. *J. Phys. Chem.* **1990**, *94*, 3265.
(35) Van Doren, J. M.; Watson, L. R.; Davidovits, P.; Worsnop, D. R.; Zahniser, M. S.; Kolb, C. E. *J. Phys. Chem.* **1991**, *95*, 1684.
(36) Hanson, D. R.; Ravishankara, A. R.; Lovejoy, E. R. *J. Geophys. Res.* **1996**, *101*, 9063.
(37) Sugiyama, M.; Koda, S.; Morita, A. *Chem. Phys. Lett.* **2002**, in press.
(38) Morita, A.; Sugiyama, M.; Koda, S. *J. Phys. Chem.* Submitted for publication, 2002.
(39) **Note**: In our earlier work, the symbol Γ_{sol} was used to take into account the effects on the uptake of Henry's law solubility. The subscript "sol" caused some confusion since it is also used to designate the solvation rate k_{sol}. The solvation process is independant of the uptake limitation due to solubility that is taken into account by the Γ coefficient. We have therefore changed the subscript of this symbol to Γ_{sat}.
(40) Worsnop, D. R.; Zahniser, M. S.; Kolb, C. E.; Gardner, J. A.; Watson, L. R.; Van Doren, J. M.; Jayne, J. T.; Davidovits, P. *J. Phys. Chem.* **1989**, *93*, 1159.
(41) Apelblat, A. *Ber. Bunsen-Ges. Phys. Chem.* **1983**, *87*, 2.
(42) Reid, R. C.; Prausnitz, J. M.; Poling, B. E. *The Properties of Gases and Liquids*; MacGraw Hill: New York, 1987.
(43) Swartz, E.; Shi, Q.; Davidovits, P.; Jayne, J. T.; Worsnop, D. R.; Kolb, C. E. *J. Phys. Chem.* **1999**, *103*, 8824.
(44) Davidovits, P.; Jayne, J. T.; Duan, S. X.; Worsnop, D. R.; Zahniser, M. S.; Kolb, C. E. *J. Phys. Chem.* **1991**, *95*, 6337.
(45) Saecker, M. E.; Nathanson, G. M. *J. Phys. Chem.* **1993**, *99*, 7056.
(46) Nathanson, G. M.; Davidovits, P.; Worsnop, D. R.; Kolb, C. E. *J. Phys. Chem.* **1996**, *100*, 13007.
(47) Ben-Naim, A.; Marcus, Y. *J. Chem. Phys.* **1984**, *15*, 2016.
(48) *Physical and the thermodynamic properties of pure chemicals: data compilation*; Daubert, T. E., Danner, R. P., Eds.; Hemisphere Publishing Corporation: New York, 1989.
(49) Zhang, H. Z.; Li, Y. Q.; Davidovits, P.; Williams, L. R.; Jayne, J. T.; Kolb, C. E.; Worsnop, D. R. *J. Phys. Chem. A* **2003**, *107*, 6398.
(50) Ishida, K.; Mori, Y. *Int. Commun. Heat Mass Transfer* **1996**, *23*, 907.
(51) DeBolt, S. E.; A., K. P. *J. Am. Chem. Soc.* **1995**, *117*, 5316.
(52) Iwahashi, M.; Hayashi, Y.; Hachiya, N.; Matsuzawa, H.; Kobayashi, H. *J. Chem. Soc., Faraday Trans.* **1993**, *89*, 707.
(53) Dallas, A. J.; Carr, P. W. *J. Chem. Soc., Perkin Trans.* **1992**, *2*, 2155.